

Genome-wide DNA methylation analysis in pediatric acute myeloid leukemia

Genki Yamato,^{1,2,*} Tomoko Kawai,^{3,*} Norio Shiba,⁴ Junji Ikeda,⁴ Yusuke Hara,² Kentaro Ohki,⁵ Shin-Ichi Tsujimoto,⁴ Taeko Kaburagi,¹ Kenichi Yoshida,⁶ Yuichi Shiraishi,⁷ Satoru Miyano,^{8,9} Nobutaka Kiyokawa,⁵ Daisuke Tomizawa,¹⁰ Akira Shimada,¹¹ Manabu Sotomatsu,¹ Hirokazu Arakawa,² Souichi Adachi,¹² Takashi Taga,¹³ Keizo Horibe,¹⁴ Seishi Ogawa,^{6,15,16} Kenichiro Hata,³ and Yasuhide Hayashi^{1,17}

¹Department of Hematology/Oncology, Gunma Children's Medical Center, Shibukawa, Japan; ²Department of Pediatrics, Gunma University Graduate School of Medicine, Maebashi, Japan; ³Department of Maternal-Fetal Biology, National Research Institute for Child Health and Development, Tokyo, Japan; ⁴Department of Pediatrics, Yokohama City University Graduate School of Medicine, Yokohama, Japan; ⁵Department of Pediatric Hematology and Oncology Research, National Research Institute for Child Health and Development, Tokyo, Japan; ⁶Department of Pathology and Tumor Biology, Graduate School of Medicine, Kyoto University, Kyoto, Japan; ⁷Division of Cellular Signaling, National Cancer Center Research Institute, Tokyo, Japan; ⁸Laboratory of DNA Information Analysis, and ⁹Laboratory of Sequence Analysis, Human Genome Center, Institute of Medical Science, University of Tokyo, Tokyo, Japan; ¹⁰Children's Cancer Center, National Center for Child Health and Development, Tokyo, Japan; ¹¹Department of Pediatrics, Jichi Medical University, Shimotsuke, Japan; ¹²Department of Human Health Sciences, Graduate School of Medicine, Kyoto University, Kyoto, Japan; ¹³Department of Pediatrics, Shiga University of Medical Science, Ōtsu, Japan; ¹⁴Clinical Research Center, National Hospital Organization Nagoya Medical Center, Nagoya, Japan; ¹⁵Center for Hematology and Regenerative Medicine, Department of Medicine, Karolinska Institute, Stockholm, Sweden; ¹⁶Institute for the Advanced Study of Human Biology, Kyoto University, Kyoto, Japan; and ¹⁷Institute of Physiology and Medicine, Jobu University, Takasaki, Japan

Key Points

- *FLT3*-ITD and high *PRDM16* expression induced methylation changes at STAT5 and AP-1 binding sites in pediatric AML.
- Hypomethylated regions in *PRDM16*-highly expressed AMLs were correlated with enhanced chromatin accessibilities at multiple genomic regions.

We investigated genome-wide DNA methylation patterns in 64 pediatric patients with acute myeloid leukemia (AML). Based on unsupervised clustering with the 567 most variably methylated cytosine guanine dinucleotide (CpG) sites, patients were categorized into 4 clusters associated with genetic alterations. Clusters 1 and 3 were characterized by the presence of known favorable prognostic factors, such as *RUNX1-RUNX1T1* fusion and *KMT2A* rearrangement with low *MECOM* expression, and biallelic *CEBPA* mutations (all 8 patients), respectively. Clusters 2 and 4 comprised patients exhibiting molecular features associated with adverse outcomes, namely internal tandem duplication of *FLT3* (*FLT3*-ITD), partial tandem duplication of *KMT2A*, and high *PRDM16* expression. Depending on the methylation values of the 1243 CpG sites that were significantly different between *FLT3*-ITD⁺ and *FLT3*-ITD⁻ AML, patients were categorized into 3 clusters: A, B, and C. The STAT5-binding motif was most frequently found close to the 1243 CpG sites. All 8 patients with *FLT3*-ITD in cluster A harbored high *PRDM16* expression and experienced adverse events, whereas only 1 of 7 patients with *FLT3*-ITD in the other clusters experienced adverse events. *PRDM16* expression levels were also related to DNA methylation patterns, which were drastically changed at the cutoff value of *PRDM16/ABL1* = 0.10. The assay for transposase-accessible chromatin sequencing of AMLs supported enhanced chromatin accessibility around genomic regions, such as *HOXB* cluster genes, *SCHIP1*, and *PRDM16*, which were associated with DNA methylation changes in AMLs with *FLT3*-ITD and high *PRDM16* expression. Our results suggest that DNA methylation levels at specific CpG sites are useful to support genetic alterations and gene expression patterns of patients with pediatric AML.

Submitted 27 May 2021; accepted 20 December 2021; prepublished online on *Blood Advances* First Edition 10 January 2022; final version published online 27 May 2022. DOI 10.1182/bloodadvances.2021005381.

*G.Y. and T. Kawai contributed equally to this study.

DNA methylation data are available at National Center for Biotechnology Information Gene Expression Omnibus under accession #GSE133986 (<https://www.ncbi.nlm.nih.gov/geo/query/acc.cgi?acc=GSE133986>).

Requests for data sharing may be submitted to Yasuhide Hayashi (hayashiy@jobu.ac.jp).

The full-text version of this article contains a data supplement.

© 2022 by The American Society of Hematology. Licensed under Creative Commons Attribution-NonCommercial-NoDerivatives 4.0 International (CC BY-NC-ND 4.0), permitting only noncommercial, nonderivative use with attribution. All other rights reserved.

Introduction

Acute myeloid leukemia (AML) is a clinically and biologically heterogeneous hematologic malignancy that is characterized by cytogenetic abnormalities, including fusion genes, mutations, epigenetic modifications, and dysregulated gene expression.^{1,2} For example, the strong expression levels of *MECOM* (also known as *EVI1*) and its homolog, *PRDM16* (also known as *MEL1*), have been reported to be associated with inferior outcomes in our pediatric patients with AML.^{3,4} Because of this genetic heterogeneity, accurate prognostic predictions for patients with AML are difficult to obtain. Therefore, novel biomarkers are needed to elucidate the clinical characteristics of patients with this clinically heterogeneous disease.

Aberrant DNA methylation has been detected in adult patients with AML, and particular methylation patterns have been associated with cytogenetic abnormalities and prognosis.⁵⁻⁸ However, only a few reports have discussed the influence of DNA methylation status on the clinical features of pediatric AML,⁹ and the significance of this potential biomarker remains unclear. Most previous studies have analyzed only the DNA methylation status of promoter regions, although some reports suggest the importance of DNA methylation in other regions, particularly in the gene body.^{10,11} In contrast to gene expression analysis, DNA methylation analysis is considered highly credible because it provides excellent quantitative determinations and absolute values, without requiring endogenous controls. Therefore, we analyzed genome-wide DNA methylation in 64 pediatric patients with AML to reveal the differences in DNA methylation patterns among various cytogenetic alterations, particularly in *PRDM16* expression value, and investigate the associations of methylation patterns with other genetic alterations.

Patients and methods

Patients

A total of 64 pediatric patients with de novo AML (age range, 0-17 years) treated in the Japanese AML-05 trial were enrolled in this study. The AML-05 trial was conducted by the Japanese Pediatric Leukemia/Lymphoma Study Group between November 2006 and December 2010 (registered at <http://www.umin.ac.jp/ctr/index.htm> as #UMIN00000511), and details of the treatment were described in another report.¹² The clinical characteristics of the 64 patients are shown in supplemental Table 1. All treatment methods, data, and sample collection protocols in the clinical trial were approved by the institutional review board of each participating institution, and written informed consent was obtained from all patients or their parents/guardians. This study was conducted in accordance with the Declaration of Helsinki and was approved by the institutional review board of Gunma Children's Medical Center, Yokohama City University Hospital, and the ethical review board of the Japanese Pediatric Leukemia/Lymphoma Study Group.

DNA methylation analysis

All leukemic samples were obtained from bone marrow at diagnosis and were cell preserved using Ficoll separation where blast cells were enriched. DNA samples from all 64 pediatric patients with AML were prepared using the ALLPrep DNA/RNA Mini Kit (Qiagen, Hilden, Germany). After adjusting the concentration of each DNA sample to 250 ng/ μ L, a comprehensive DNA methylation analysis

was performed using the Infinium MethylationEPIC BeadChip (Illumina, San Diego, CA) according to the manufacturer's protocol. Methylation data were obtained in an IDAT file format with the iScan System (Illumina) and then processed using the RnBeads package (<https://bioconductor.org/biocLite.R>)¹³ in R software (version 3.4.3). The data were normalized using the Illumina method in the RnBeads package, and the manifest file was annotated using IlluminaHumanMethylationEPICanno.ilm10b2.hg19. We removed 3828 unreliable probes by using a greedy approach, as well as 2932 non-cytosine guanine dinucleotide (CpG) targeting probes. We also filtered 18 926 probes located on the X or Y chromosome and 17 240 single nucleotide polymorphism-related probes. Finally, we obtained 757 561 autosomal probes from 64 samples. We classified DNA methylation levels into 3 groups according to their β value: hypermethylation (≥ 0.67), intermediate methylation (0.34-0.66), and hypomethylation (≤ 0.33), respectively.

Assay for transposase-accessible chromatin sequencing

We performed an assay for transposase-accessible chromatin sequencing (ATAC-seq) using 5 other samples from pediatric patients with AML who were not registered in the AML-05 study but were treated at Yokohama City University Hospital (supplemental Table 2).

Cells were harvested and frozen in culture media containing CELL-BANKER 1 (ZENOAQ, Fukushima, Japan). Cryopreserved cells were sent to Active Motif to perform ATAC-seq. The cells were then thawed in a 37°C water bath, pelleted, washed with cold phosphate-buffered saline, and tagmented as previously described,¹⁴ with some modifications based on Corces et al.¹⁵ Briefly, cell pellets were resuspended in lysis buffer, pelleted, and tagmented using the enzyme and buffer provided in the Nextera Library Prep Kit (Illumina). Tagmented DNA was then purified using the MinElute PCR Purification Kit (Qiagen), amplified with 10 cycles of polymerase chain reaction (PCR), and purified using Agencourt AMPure SPRI Beads (Beckman Coulter). Resulting material was quantified using the KAPA Library Quantification Kit for Illumina platforms (KAPA Biosystems) and sequenced with PE42 sequencing on the NextSeq 500 Sequencer (Illumina).

Reads were aligned using the Burrows-Wheeler Aligner algorithm (MEM mode; default settings). Duplicate reads were removed; only reads mapping as matched pairs and only uniquely mapped reads (mapping quality ≥ 1) were used for further analysis. Alignments were extended in silico at their 3' ends to a length of 200 bp and assigned to 32-nt bins along the genome. The resulting histograms (genomic signal maps) were stored in bigWig files.

Screening for molecular characterization

The molecular characterization included mutational analyses of internal tandem duplication of *FLT3* (*FLT3-ITD*), *NPM1* (exon 12), *WT1* (exons 7-10), and all coding regions of *CEBPA*, *DNMT3A*, *TET2*, and *IDH1/2*¹⁶⁻²²; gene rearrangement analyses of *KMT2A*, *RUNX1-RUNX1T1*, *CBFB-MYH11*, *NUP98-NSD1*, and *FUS-ERG* (reverse transcription PCR); and an analysis of *KMT2A* partial tandem duplication (multiplex ligation-dependent probe amplification methods).^{23,24} GeneScan (Applied Biosystems, Tokyo, Japan) was used to determine the allele ratio of *FLT3-ITD* to the wild-type alleles; here, allele ratio values of >0.7 and ≤ 0.7 were defined as high and low, respectively, according to a previous report.²⁵ We also

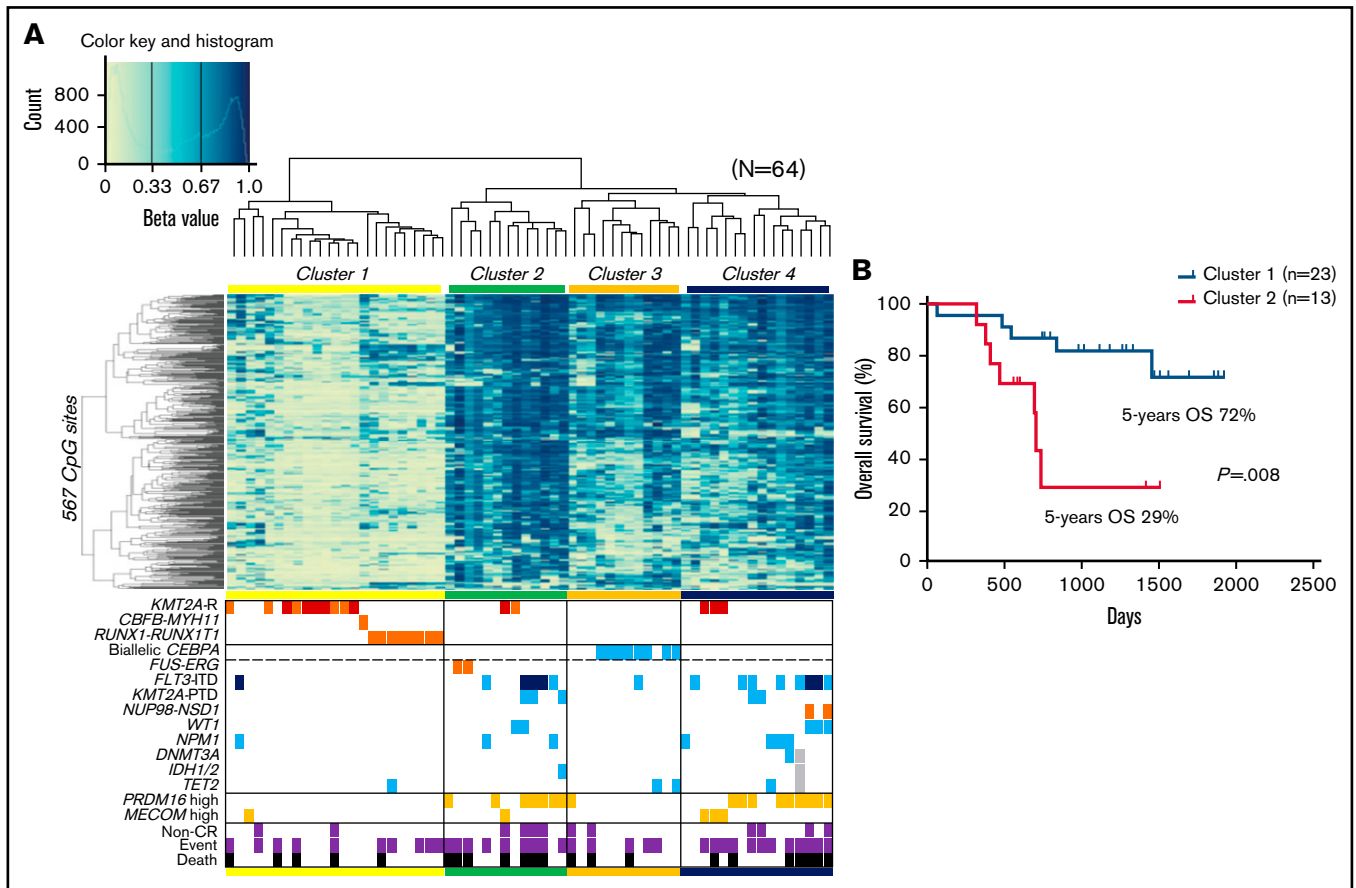


Figure 1. Unsupervised hierarchical clustering of DNA methylation profiles and associations between DNA methylation clusters and additional parameters. (A) Heatmap of the DNA methylation profiles of 64 AMLs based on unsupervised hierarchical clustering. Clustering was based on the 567 CpG sites with the most variable methylation values in the 64 studied cases. Four clusters were generated: 1, 2, 3, and 4. DNA methylation levels were classified into 3 groups according to their β value: hypermethylation (≥ 0.67), intermediate methylation (0.34-0.66), and hypomethylation (≤ 0.33), respectively. Light blue, orange, and dark orange indicate the presence of the specified mutation, high gene expression, and chromosomal aberration, respectively. Brown indicates *KMT2A-MLL3* fusion, and dark blue indicates *FLT3-ITD* with high allele ratio (>0.7). Purple and black indicate non-complete remission (CR) and events and deaths, respectively. (B) Comparison of the Kaplan-Meier curves of OS between clusters 1 and 2. *KMT2A-R*, *KMT2A* rearrangement; PTD, partial tandem duplication.

performed quantitative reverse transcription PCR analysis of *PRDM16* and *MECOM* expression and defined the following respective cutoff points according to the results of receiver operating characteristic curve in the previous report: *PRDM16/ABL1* ratio ≥ 0.10 and *MECOM/ABL1* ratio ≥ 0.10 .³

Transcriptome analysis

We performed transcriptome analysis in 45 of 64 patients to investigate the relationship between DNA methylation patterns and gene expression, which was performed according to the methods described in a previous report.²⁶

Transcription factor-binding site analysis

Transcription factor (TF) motifs were found by HOMER (version 4.11) with Finding Enriched Motifs in Genomic Regions using the default setting.²⁷

Use of a public database

We compared the DNA methylation data and expression data of our cohort with those of the National Cancer Institute TARGET

cohort in the public database. The public data included 91 pediatric patients with AML analyzed using a 450K methylation array. Of these, only 8 cases had expression data. The public database was available at <https://target-data.nci.nih.gov/Public/AML/>.

Statistical methods

All statistical analyses were performed using EZR software (version 1.36; Saitama Medical Center, Jichi Medical University, Saitama, Japan).²⁸ All *P* values were 2 tailed, and a *P* value $<.05$ was considered statistically significant. Detailed statistical methods are described in the data supplement. Analysis of variance was used to assess the differences between groups in mean age and white blood cell count at diagnosis. The χ^2 test was applied to comparisons of other factors. Overall survival (OS) and event-free survival (EFS) outcomes were estimated using the Kaplan-Meier method, and differences in survival were compared using the log-rank test. OS was defined as the time interval from diagnosis to death or last follow-up, whereas EFS was defined as the time interval from diagnosis to the date of treatment failure (induction failure, relapse, second malignancy, or death) or the date of last contact, whichever was appropriate. For methylation analysis, *P* values were determined

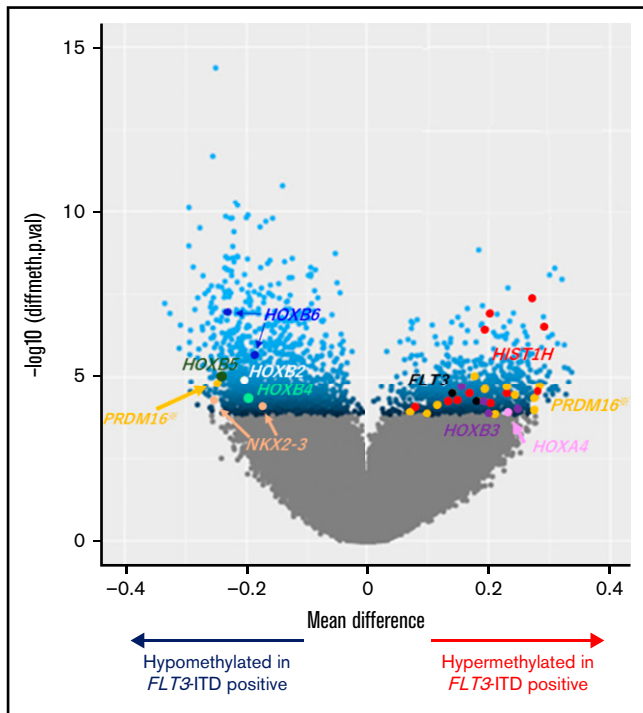


Figure 2. Volcano plot comparing the number of significantly hyper- and hypomethylated probes in patients with *FLT3*-ITD. Mean methylation differences (x-axis) and negative log₁₀-transformed statistical *P* values (y-axis) between AML with and without *FLT3*-ITD are shown in the volcano plot. Methylation levels of the 2501 CpG sites were significantly different between the groups at false discovery rate-adjusted *P* values <.05, which are represented in blue. Dots in other colors correspond to various genes as follows: brown, *NKX2-3*; white, *HOXB2*; aquamarine, *HOXB4*; green, *HOXB5*; cyan, *HOXB6*; black, *FLT3*; red, *HIST1H* genes (including *HIST1H2AE*, *HIST1H2AJ*, *HIST1H2BG*, *HIST1H2BI*, *HIST1H3E*, and *HIST1H3J*); orange, *PRDM16*; purple, *HOXB3*; and pink, *HOXA4*. Among the 12 dots of *PRDM16*, 1 CpG site appeared on the hypomethylation side located near the TSS of *PRDM16*. In contrast, the remaining 11 CpG sites appeared on the hypermethylation side located in the *PRDM16* gene body.

using a 2-sided Welch's *t* test, and a false discovery rate-adjusted *P* value <.05 was considered statistically significant. Clustering was performed using the complete linkage method. CpG-associated genes were determined by the Genomic Regions Enrichment of Annotations Tool (GREAT [version 4.0.4]) if transcription start sites (TSSs) were located between 1 megabase upstream or downstream of the concerned CpG. Significant terms were selected when the false discovery rate-adjusted *P* value was <.05 by both binomial and hypergeometric tests.

Results

Clustering in the DNA methylation analysis was consistent with molecular features

We analyzed 757 561 methylation sites per sample, collected from our cohort of 64 pediatric patients with AML. To identify the differences in DNA methylation across samples, we selected 567 CpG sites that showed the most variable methylation values among 64 AMLs (standard deviation >0.3; supplemental Table 3). An unsupervised hierarchical clustering analysis based on the methylation

values at these sites generated 4 clusters of AML (clusters 1-4; Figure 1A). Clusters 1 and 2 consisted of AMLs that exhibited lowest and highest methylation levels, respectively. Clusters 3 and 4 corresponded to intermediate methylation levels. Cluster 2 had a significantly worse OS than cluster 1 (*P* = .008; Figure 1B). Distributions of *FLT3*-ITD and high *PRDM16* expression were significantly unequal (*P* = .003 and *P* < .001, respectively), with high frequencies in clusters 2 and 4 and low frequencies in clusters 1 and 3. Patients in clusters 2 and 4 tended to be older and have a higher white blood cell count at diagnosis and a higher mortality rate than patients in clusters 1 and 3 (supplemental Table 4). Cluster 1 was characterized by the presence of known favorable prognostic factors, such as *RUNX1-RUNX1T1* fusion and *KMT2A* rearrangement with low *MECOM* expression.²⁹ All patients with biallelic *CEBPA* mutations, which indicated a favorable outcome, were classified under cluster 3. Unsupervised hierarchical clustering with methylation values of CpG sites that showed the most variable methylation values among our 64 AMLs succeeded in dividing biallelic *CEBPA* mutations and *RUNX1-RUNX1T1* fusion in publicly available TARGET data (supplemental Figure 1).

DNA methylation patterns predicted the outcomes of patients with *FLT3*-ITD

Unsupervised hierarchical clustering divided patients with AML with *FLT3*-ITD and/or high *PRDM16* expression into clusters 2 and 4 (Figure 1A). Therefore, we sought CpG sites with methylation values that differed significantly between patients with and without *FLT3*-ITD. Consequently, we identified significantly different methylation values at 2501 CpG sites in patients with *FLT3*-ITD, in comparison with others. The hypermethylation of *HOXB3* (5' untranslated region [UTR]), *HOXA4* (TSS200), *FLT3* (body), and *PRDM16* (body) and the hypomethylation of *HOXB2* (TSS1500), *HOXB4* (TSS1500), *HOXB5* (TSS1500, TSS200, body, and 3' UTR), *HOXB6* (TSS200, body, and 3' UTR), and *NKX2-3* (body and 3' UTR) were observed in patients harboring *FLT3*-ITD (Figure 2). Patients with *FLT3*-ITD showed a significantly higher expression of *FLT3* than those without *FLT3*-ITD (*P* = .022; supplemental Figure 2). This result was consistent with a previous report that demonstrated that hypermethylation of the gene body was associated with high gene expression.³⁰ Furthermore, 11 CpG sites located in *HIST1H* that regulate the transcription of individual genes by bundling histone octamers via DNA methylation exhibited significant hypermethylation in patients harboring *FLT3*-ITD (Figure 2). The *HOX* family of genes is reported to be expressed in *FLT3*-ITD/*NPM1*-specific TF networks.³¹ Depending on the methylation values of the 1243 CpG sites that were significantly different between *FLT3*-ITD⁺ and *FLT3*-ITD⁻ AMLs, patients were categorized into 3 clusters (Figure 3A). Cluster A was composed of 8 patients carrying *FLT3*-ITD, and 4 patients harbored the *WT1* mutation. The remaining 7 of the 15 patients with *FLT3*-ITD were distributed in cluster B or C. All 8 patients with *FLT3*-ITD⁺ in cluster A experienced events, whereas only 1 of 7 patients with *FLT3*-ITD⁺ in cluster B or C experienced events (Figure 3A; Table 1). According to the survival analysis between patients with *FLT3*-ITD in clusters A and B or C, patients in cluster A showed worse prognosis than those in the other clusters (5-year OS, 13% vs 100%; *P* = .002 and 5-year EFS, 0% vs 86%; *P* < .001; Figure 3B-C). Remarkably, all patients in cluster A expressed high levels of *PRDM16* (Figure 3A). High *PRDM16*

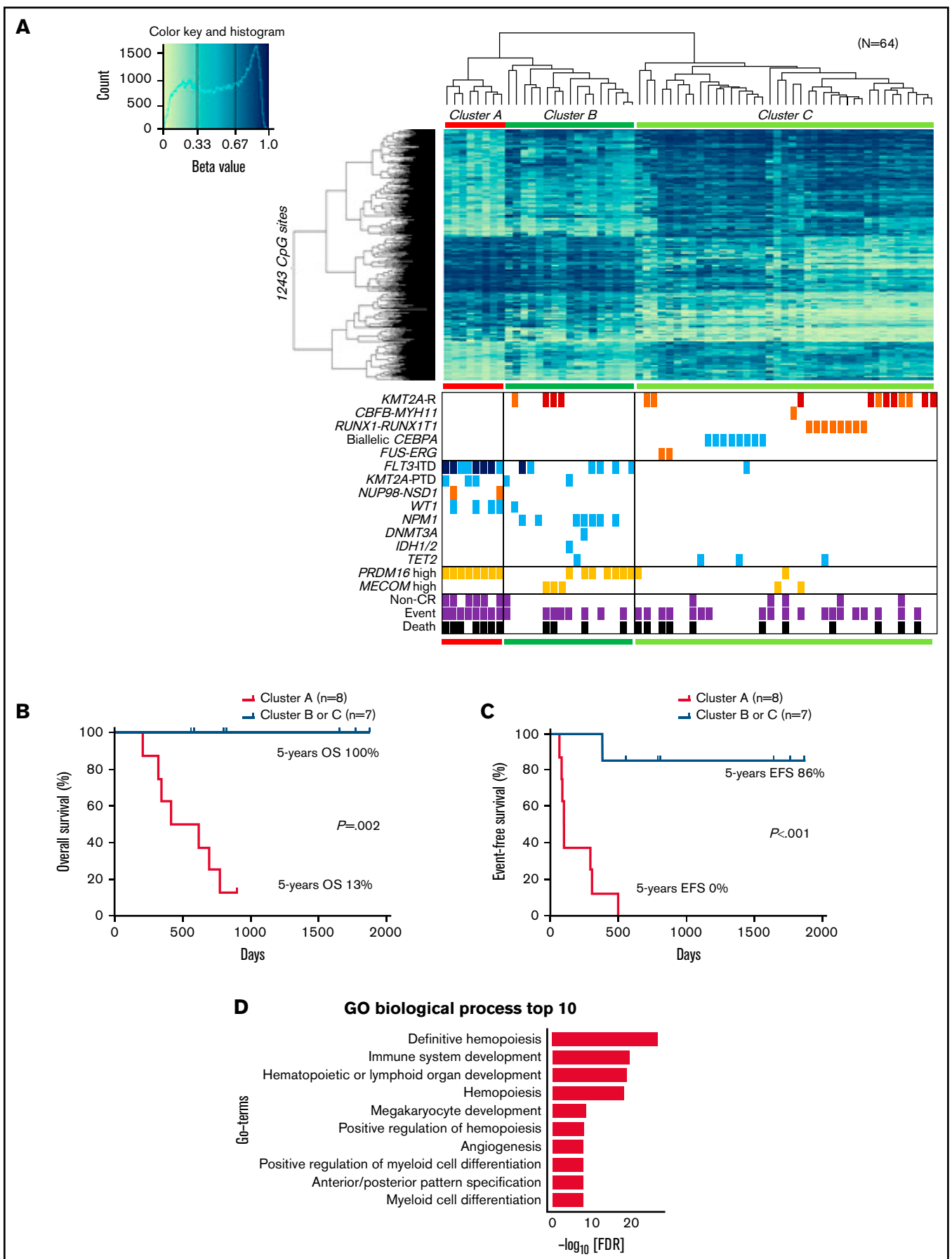


Figure 3. Clustering of DNA methylation profiles according to *FLT3-ITD*. (A) hierarchical clustering analysis with the methylation levels of the 1243 CpG sites with methylation differences of $\geq 20\%$ generated 3 clusters (A, B, and C), and associations of the DNA methylation cluster according to *FLT3-ITD* status with mutations,

expression was significantly more frequent in cluster A than in clusters B ($P = .023$) and C ($P < .001$).

The 1243 CpG sites in Figure 3A were allocated to 1481 genes and revealed that these genes were significantly enriched in definitive hemopoiesis and had the lowest P values (Figure 3D; supplemental Table 5). The 9 terms with the next lowest P values were nearly related to lymphocyte, hemopoiesis, and myeloid (Figure 3D). Some of them overlapped with the top enriched gene ontology terms for upregulated genes of *FLT3-ITD* compared with $CD34^+$ peripheral blood stem cells, which have been reported previously.³¹

Three TF-binding motifs were significantly enriched in the 1243 CpG sites (Figure 4A). Methylation levels at the 135 CpG sites, near where the top *STAT5* motifs were, classified the 8 patients of cluster A in the first trunk (Figure 4B). Of the 135 CpG sites, 85% were located in the gene body or intergenic region (Figure 4C; supplemental Table 6), and 65% were annotated as candidate cis-regulatory elements (Figure 4D).³¹ ATAC-seq of 5 AMLs (supplemental Table 2) confirmed that genomic regions where DNA methylation changed close to *STAT5*-binding motifs were specifically opened in 2 AMLs with *FLT3-ITD* and high *PRDM16* gene expression (Figure 4E), which may indicate that the detection of aberrant *STAT5* activity implies a worse prognosis in patients with *FLT3-ITD*. In addition, high *PRDM16* expression was concentrated in cluster A, which indicated that high *PRDM16* expression may affect DNA methylation.

Cutoff values of *PRDM16* expression as defined by DNA methylation analysis

We examined the relationship between *PRDM16* expression and DNA methylation status and identified 244 CpG sites wherein methylation status was significantly associated with *PRDM16* expression level (supplemental Table 7). The arrangement of the 64 patients according to a series of *PRDM16* expression values yielded 2 groups with distinct methylation patterns (Figure 5A). The methylation pattern drastically changed at this border ($PRDM16/ABL1 = 0.10$). We evaluated various cutoff points to confirm the relationship between the methylation pattern and expression value of *PRDM16* (supplemental Figure 3), and the cutoff point we adopted was appropriate. Although the number of samples for annotation of gene expression levels was limited, we reconfirmed that methylation levels at the 244 CpG sites accurately distinguished AMLs with highly expressed *PRDM16* in the TARGET data (supplemental Figure 4). Methylation differences at the 244 CpG sites were associated with changes in expression levels, especially in the following genes, in which methylation levels at multiple CpG sites were significantly altered in *PRDM16*_high AMLs: *SCHIP1*, *HOXB-AS3*, *HOXB5*, and *RPS6KL1* (supplemental Figure 5). Figure 5B presents 30 CpG sites that were associated with particularly large differences in

direction of hypermethylation values between the 2 groups. Nine of these sites were located at *PRDM16* (supplemental Table 7). Remarkably, 1 CpG site (*PRDM16_1*) near the TSS of *PRDM16* was hypomethylated in patients highly expressing *PRDM16* (Figure 5A). In contrast, the remaining 9 CpG sites (*PRDM16_2-10*) located in the *PRDM16* gene body were hypermethylated and colocalized at polycomb repressive complex target regions (Figure 5B-C; supplemental Figure 6). Furthermore, 6 of these 9 sites were present in the 567 CpG sites that were identified as abnormal DNA methylation sites associated with OS (Figure 1). The ATAC-seq of 5 AMLs (supplemental Table 2) revealed that chromatin accessibility was enhanced only in 2 AMLs with high *PRDM16* expression at the TSS region of *PRDM16* (Figure 5C), TSS of *SCHIP1* (Figure 5D), and 22 other CpG sites (supplemental Figure 7), which were hypomethylated among the 244 CpG sites in patients with high *PRDM16* expression (Figure 5A). These opened regions occurred not only in TSSs but also in the gene body and intergenic regions (supplemental Table 7). These results revealed that molecular feature-specific hypomethylation could be a marker of enhanced chromatin accessibility in pediatric AML.

Association of DNA methylation regulation and TFs

Because we identified 17 AMLs in which methylation levels were clearly dissociated from others according to *PRDM16* expression levels (Figure 5A), we focused on the methylation levels of these 17 AMLs. Between the 17 AMLs of high *PRDM16* expression and those of low *PRDM16* expression, 4849 CpG sites were significantly different. The TF-binding motifs were significantly enriched only at 1893 hypomethylated CpG sites (supplemental Figure 8A); among the 15 significant TF motifs, the AP-1 motif was enriched (supplemental Figure 8B). Meanwhile, the *STAT5* motif was not included in the 15 significant motifs.

We confirmed that the 2 AMLs with high *PRDM16* expression analyzed by ATAC-seq specifically enhanced chromatin accessibility at the AP-1 motif for which methylation levels were significantly altered in the nearby 17 AMLs of high *PRDM16* expression; these sites were reported to be distal enhancer-like signatures (supplemental Figure 8C).³² Further analysis revealed that 8 AMLs with *FLT3-ITD* and high *PRDM16* expression in cluster A, shown in Figure 3A, significantly regulated methylation at 7629 CpG sites, $\geq 20\%$ more than those in cluster C. Again, TF-binding motifs were significantly enriched only in the hypomethylated 3180 CpG sites (supplemental Figure 9A). Among them, both AP-1 and *STAT5* motifs were included (supplemental Figure 9B). Clustering by *STAT5*- or AP-1-binding CpG sites classified AMLs with *FLT3-ITD* and high *PRDM16* expression not only in our cohort but also in the TARGET cohort (supplemental Figure 10). These results suggest that AMLs in which *FLT3-ITD* and *PRDM16* expression were high concurrently occurred with aberrant AP-1 and *STAT5* signaling. However, these 2 signals did not seem to directly explain why *FLT3-ITD* induced

Figure 3 (continued) expression levels, cytogenetic features, and outcomes in pediatric patients with AML. DNA methylation levels were classified into 3 groups according to their β value: hypermethylation (≥ 0.67), intermediate methylation (0.34-0.66), and hypomethylation (≤ 0.33), respectively. Light blue, orange, and dark orange indicate presence of the specified mutation, high gene expression, and chromosomal aberration, respectively. Brown indicates *KMT2A-MLLT3* fusion, and dark blue indicates *FLT3-ITD* with high allele ratio (>0.7). Gray and black indicate non-complete remission (CR) and events and deaths, respectively. (B-C) Comparison of the Kaplan-Meier curves of OS (B) and EFS (C) between clusters A and B or C of panel A in 15 patients with *FLT3-ITD*. (D) Gene ontology (GO) biologic process for the top 1243 CpG-related 1481 genes. FDR, false discovery rate; GO, gene ontology; *KMT2A-R*, *KMT2A* rearrangement; PTD, partial tandem duplication.

Table 1. Clinical characteristics of 15 pediatric patients with AML with *FLT3*-ITD

N	Age, y	Sex	WBC, 10 ⁹ /L	Blast, %	<i>FLT3</i> -ITD AR	Cluster	Other genetic alterations	<i>PRDM16</i> expression	Non-CR	Relapse	Outcome
G_AML_012	11.4	F	4.5	78.4	0.71	A	<i>WT1</i> , <i>KMT2A</i> -PTD	High	+	–	Dead
G_AML_136	12.8	M	7.0	76.4	0.70	A	<i>WT1</i>	High	–	+	Dead
G_AML_153	7.4	M	168.1	92	0.84	A	–	High	+	+	Dead
G_AML_188	10.8	F	380.5	88.6	0.60	A	–	High	–	+	Dead
G_AML_222	11.2	F	210.3	81.1	0.48	A	<i>NUP98-NSD1</i> , <i>WT1</i>	High	+	–	Dead
G_AML_225	17.3	M	147.9	85	0.73	A	<i>NUP98-NSD1</i> , <i>WT1</i>	High	+	+	Dead
G_AML_306	10.8	F	45.3	85.5	0.64	A	<i>KMT2A</i> -PTD	High	+	+	Alive
G_AML_381	11.8	M	70.8	87.2	4.47	A	<i>KMT2A</i> -PTD	High	+	+	Dead
G_AML_051	11.5	F	4.5	66.5	0.30	B	<i>NPM1</i>	High	–	–	Alive
G_AML_105	17.5	F	65.3	89	0.63	B	–	Low	–	–	Alive
G_AML_319	2.8	M	17.7	95.1	0.77	B	<i>NPM1</i>	Low	–	–	Alive
G_AML_329	10.6	F	4.6	44.8	0.24	B	–	High	–	–	Alive
G_AML_432	2.1	F	209.0	51.6	0.38	B	<i>NPM1</i>	Low	–	+	Alive
G_AML_437	16.9	M	8.5	23.1	0.11	B	<i>NPM1</i>	High	–	–	Alive
G_AML_018	2.7	M	114.4	79	0.34	C	–	Low	–	–	Alive

AR, allele ratio; CR, complete remission; F, female; M, male; PTD, partial tandem duplication; WBC, white blood cell.

extraordinary expression of *PRDM16* or vice versa. Neither of the TFs has been reported to bind the promoter of *PRDM16* by ENCODE reference data.³³

Cutoff values of *MECOM* expression as defined by DNA methylation analysis

We extracted 482 CpG sites that were significantly associated with *MECOM* expression and investigated the relationship between expression of this gene and DNA methylation profiles. The arrangement of 64 patients according to a series of *MECOM* expression values yielded 2 groups with distinct DNA methylation patterns (Figure 6A). Similar to *PRDM16*, the methylation pattern was drastically changed at this border (*MECOM/ABL1* = 0.10). Hierarchical clustering of methylation values of the 50 CpG sites with the smallest *P* values revealed that high *MECOM* expression was significantly associated with hypomethylation at 4 CpG sites in transcriptional repressor GATA-binding 1 (*TRPS1*), which encodes a member of the *GATA* family of transcriptional repressors (Figure 6B).³⁴ These results imply that the *PRDM16* and *MECOM* expression cutoff points³ with *PRDM16/ABL1* ratio ≥ 0.10 and *MECOM/ABL1* ratio ≥ 0.10 were associated with signature DNA methylation patterns. Moreover, specific CpG sites within the gene bodies of *PRDM16* were significant markers indicative of a high *PRDM16* expression.

Discussion

In this study, we examined genome-wide DNA methylation patterns in 64 pediatric patients with de novo AML. The unsupervised hierarchical clustering of the patients' DNA methylation status yielded 4 clusters, which correlated strongly with genetic alterations that are known to indicate AML prognosis. We observed that the hypermethylation and hypomethylation of the 567 extracted CpG sites tended to be associated with worse and better prognosis, respectively. Intriguingly, the methylation pattern of patients with AML with *KMT2A-MLL3* and low *MECOM* expression resembled that of

those harboring *RUNX1-RUNX1T1*. These findings suggest that the DNA methylation patterns may be also significant prognostic factors in pediatric AML harboring *KMT2A-MLL3* and could potentially elucidate the pathologic mechanisms of AML.

A previous report suggested that the established adverse effect of *FLT3*-ITD on survival was modulated by a cooccurring variant, such as a *WT1* or *NPM1* mutation or *NUP98-NSD1* fusion.³⁵ Patients with *FLT3*-ITD harboring a *WT1* mutation or *NUP98-NSD1* fusion have an adverse prognosis, whereas those with an *NPM1* mutation have a favorable prognosis. A similar trend was observed in the present study (Figure 3A; Table 1). Although the number of patients was limited, the DNA methylation pattern distinguished between patients with *FLT3*-ITD who harbored a *WT1* mutation or *NUP98-NSD1* fusion versus those who harbored an *NPM1* mutation. As described previously,³⁵ patients who harbored a *WT1* mutation exhibited aberrant promoter DNA hypermethylation and consequent widespread gene silencing. The prognosis of patients with *FLT3*-ITD who did not harbor these cooccurring variants could also be distinguished clearly by the DNA methylation patterns (Figure 3A). Accordingly, DNA methylation patterns might be an accurate prognostic factor for patients with *FLT3*-ITD.

Three TFs were extracted from the TF-binding site analysis for the 1243 regions in which significantly different DNA methylations were confirmed, with the lowest *P* value between AMLs with and without *FLT3*-ITD (Figure 4A). Of these, STAT5 has been reported to be an effector activated by *FLT3*-ITD, thus leading to cell proliferation and antiapoptosis.³⁶ Furthermore, *FLT3*-ITD has been reported to be linked to a distinct DNA methylation signature targeting STAT sites.³⁷ Next, we investigated CpG sites that showed significantly different methylation statuses between *PRDM16*_{high} (red) and *PRDM16*_{low} (green) AMLs, shown in Figure 5A. The STAT5-binding sites do not seem to correlate with high expression of *PRDM16* (supplemental Figure 8A-B). Instead, the AP-1-binding motif was involved in high *PRDM16* expression. Finally, AMLs harboring *FLT3*-ITD concomitant with high *PRDM16* expression

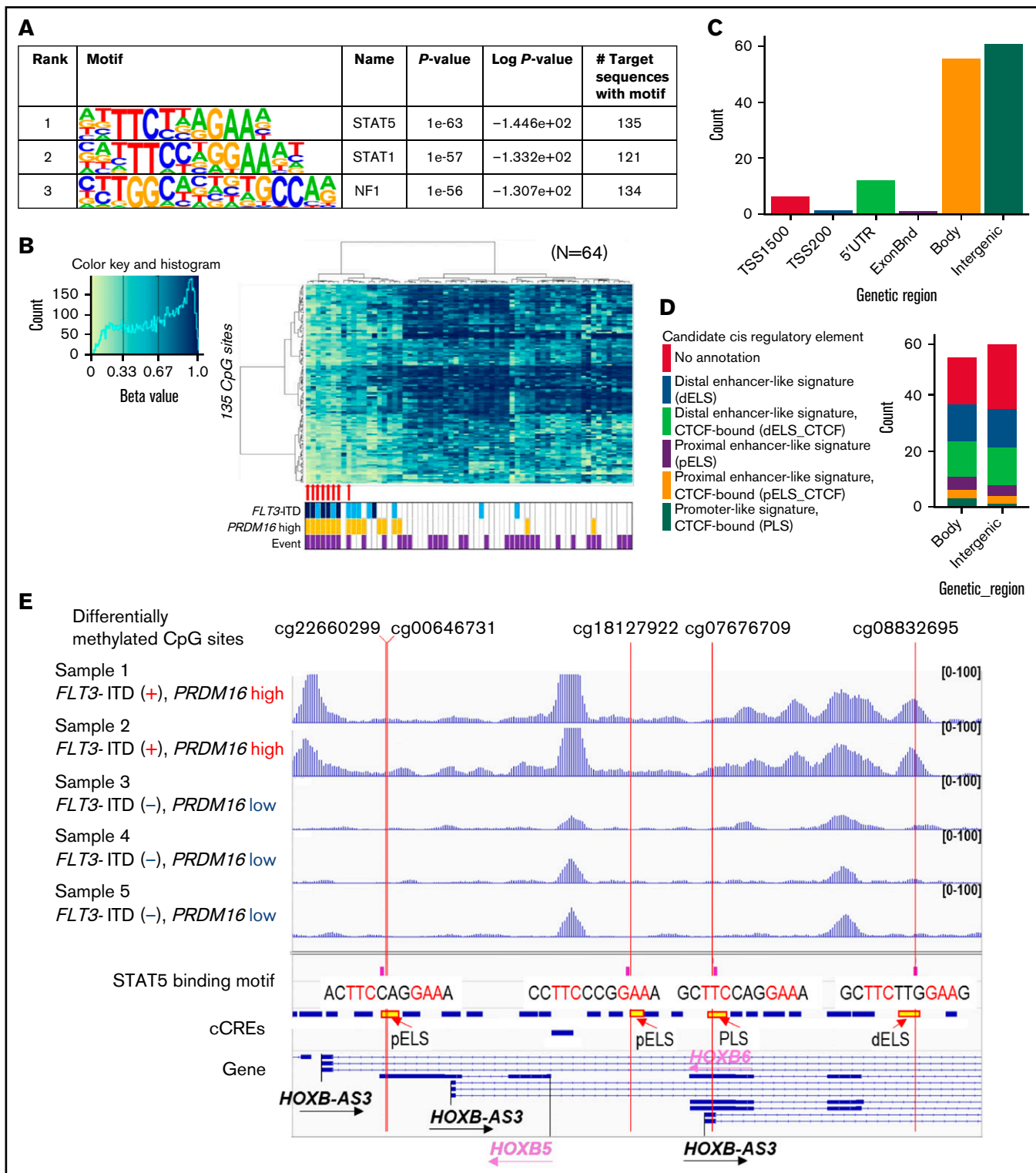


Figure 4. TF-binding motif analysis of genomic regions in which DNA methylation was different between *FLT3-ITD*⁺ and *FLT3-ITD*⁻ AMLs. (A) The 3 TFs were confirmed by HOMER in the genomic regions ± 200 bp in length adjacent to each of the 1243 CpG sites with a P value $< 1e-50$. (B) hierarchical clustering of methylation levels at 135 CpG sites in the STAT5-binding sites was classified in 8 patients of cluster A in the first trunk. Eight patients with AML with *FLT3-ITD* in cluster A in Figure 3A are indicated by red arrows. (C) Genetic localization of 135 CpG sites for which the STAT5-binding motif existed nearby. (D) Annotation of candidate cis-regulatory elements (cCREs) in the gene body and intergenic CpG sites close to STAT5-binding motifs. (E) Chromatin accessibility of the genomic regions where STAT5 binds close to the methylation-changed CpG sites was analyzed in 5 patients using ATAC-seq. Some open chromatin regions in the *HOXB-AS3* gene were identified only in patients with *FLT3-ITD* and high *PRDM16* gene expression. Annotations of cCREs are described in panel D.

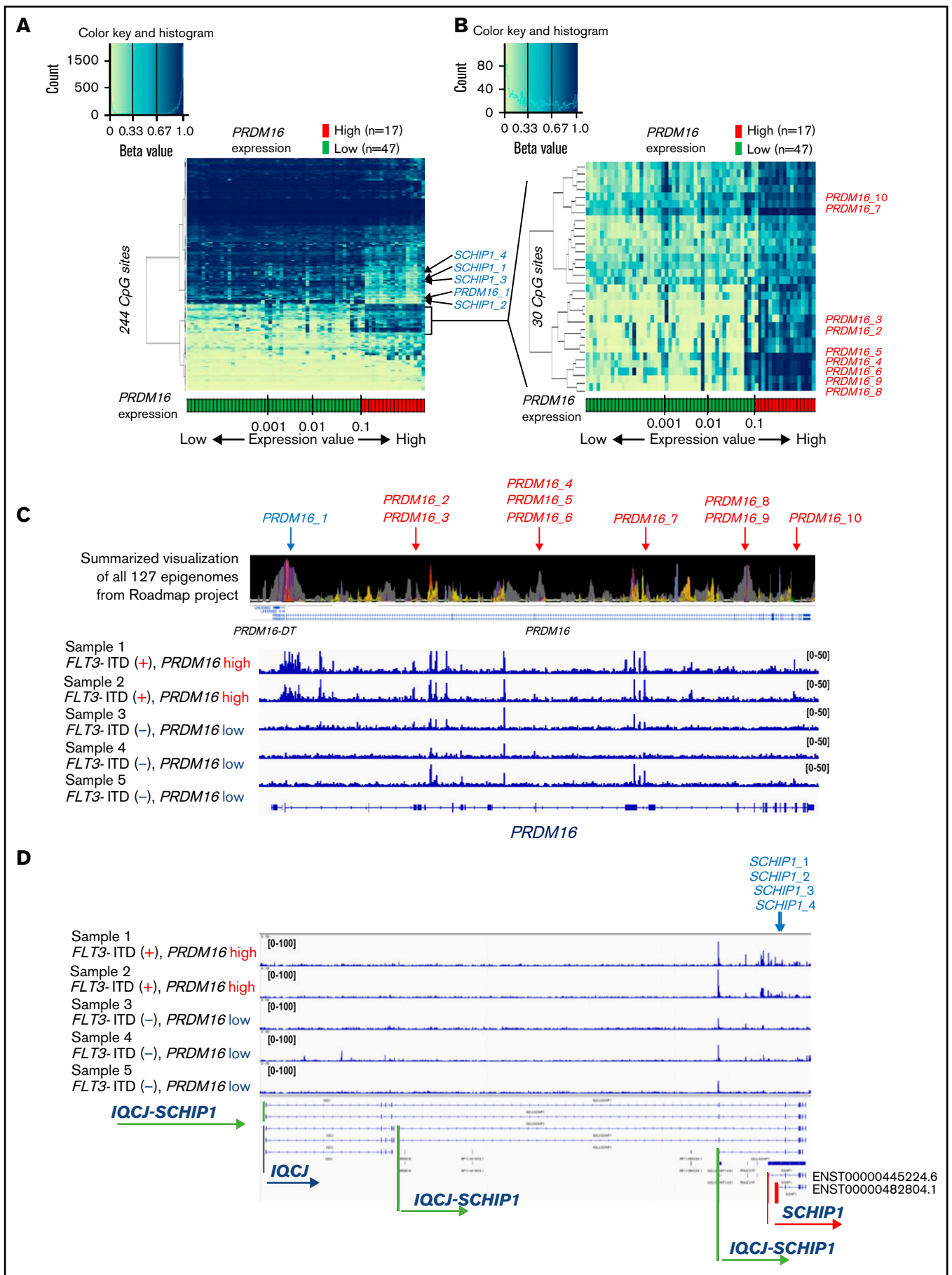


Figure 5. Strong associations of DNA methylation profiles with PRDM16 expression. (A) Heatmap of the DNA methylation profiles based on the methylation values of 244 CpG sites associated with PRDM16 expression. Arrangement of the 64 patients according to a series of PRDM16 expression values (more rightward column

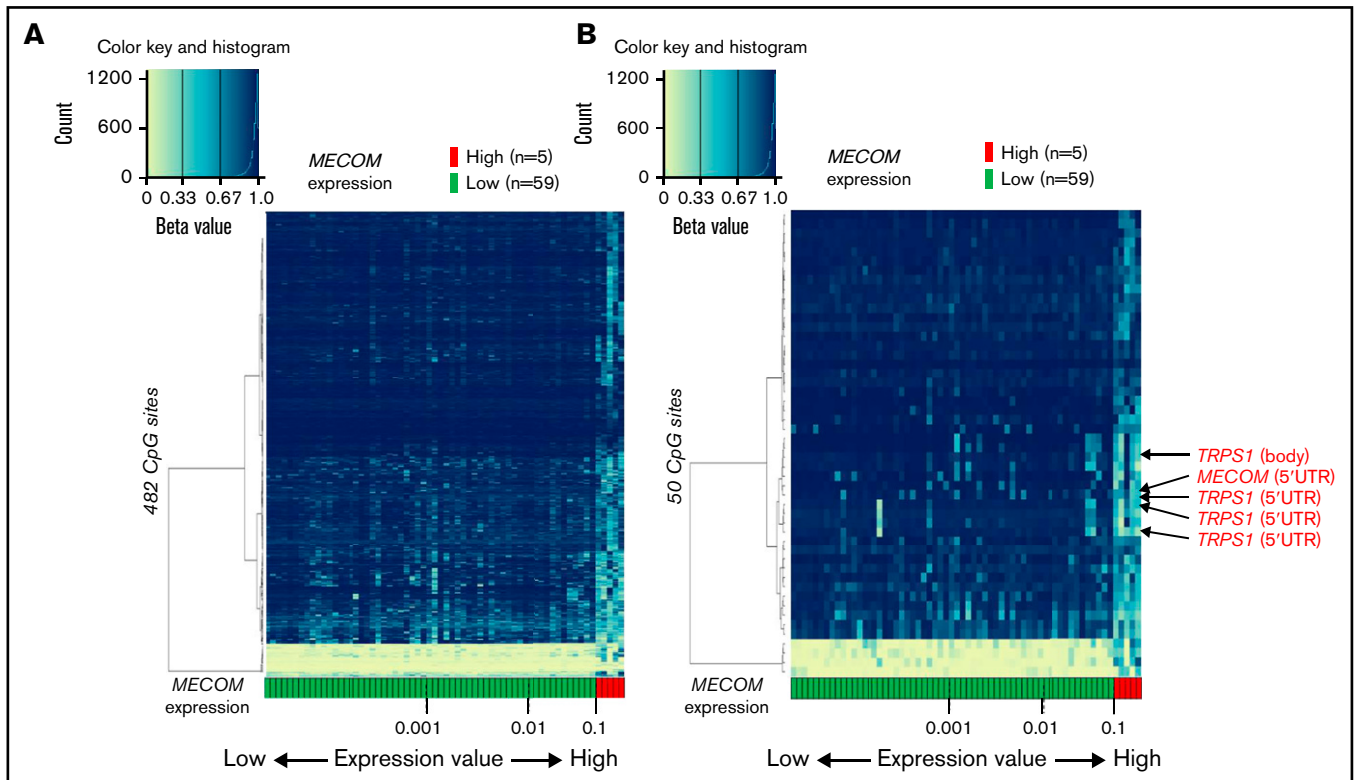


Figure 6. Association of DNA methylation profiles with *MECOM* expression. (A) Heatmap of DNA methylation profiles according to the methylation values at the 482 CpG sites associated with *MECOM* expression. Arrangement of 64 patients according to a series of *MECOM* expression values (more rightward column location indicates stronger *PRDM16* expression) yielded 2 groups with distinct methylation patterns. This classification substantially distinguished patients with high and low *MECOM* expression (left). (B) Heatmap of 50 CpG sites associated with particularly large differences in methylation values between patients with high and low *MECOM* expressions (right).

included STAT5- and AP-1-binding motifs in nearby altered DNA methylation CpG sites (supplemental Figure 9). We reconfirmed these results in the TARGET cohort (supplemental Figure 10). Therefore, methylation levels at STAT5- and AP-1-binding sites may correlate with high expression of *PRDM16* with *FLT3-ITD*, synergistically.

We previously identified high levels of *PRDM16* expressions as a poor prognostic factor in pediatric AML.^{3,4} In this study, we revealed that highly expressed *PRDM16* in AML exhibited significant hypermethylation within the *PRDM16* gene body at 9 CpG sites with polycomb repressive complex target regions (Figure 5C). It was only these 9 that methylation was significantly changed within 614 array probes of *PRDM16* genes. These results indicated that significant methylation changes at the 9 CpG sites were markers for estimating the degree to which *PRDM16* expression levels were related to AML methylome aberrance. *PRDM16* is highly homologous to *MDS1/EVI1*, which is an alternatively spliced transcript of *MECOM*,³⁸ and both *PRDM16* and *MECOM* encode histone H3 lysine 9

monomethyltransferases, which maintain heterochromatin integrity.³⁹ Recent reports have demonstrated the distinct roles for Prdm16 isoforms.^{40,41} We revealed that methylation at the 4 CpG sites near the alternative TSS of *SCHIP1* (ENST00000482804.1) clearly decreased in AMLs with highly expressed *PRDM16* concomitantly with enhanced chromatin accessibility and increased transcript levels. Two of the 4 CpG sites at *SCHIP1* were included in the 1243 CpG sites that were differentially methylated, with >20% between *FLT3-ITD*⁺ and *FLT3-ITD*⁻. It is impossible to discriminate between the effects of *FLT3-ITD* and *PRDM16* high expression on the changes in DNA methylation in our study. *SCHIP1* encodes a cytoskeletal protein and is identified as an intermediate early gene controlled by PDGF signaling.^{42,43} PDGF receptors and FLT3 are both type 3 receptor tyrosine kinases. Gene rearrangements of *PDGFRA* and *PDGFRB* have been reported in AML.^{44,45} Additional molecular aberrations or cross talk between PDGFR and FLT3 might be involved in DNA methylation changes.

Figure 5 (continued) location indicates stronger *PRDM16* expression) yielded 2 groups with distinct methylation patterns. This classification substantially distinguished patients with high and low *PRDM16* expression. (B) Heatmap of 30 CpG sites associated with particularly large differences in methylation values between patients with high and low *PRDM16* expressions. (C) Chromatin state annotations for the *PRDM16* gene across 127 reference epigenomes based on the National Institutes of Health Roadmap project and chromatin accessibility of the *PRDM16* gene in 5 patients with pediatric AML. Chromatin status is indicated by color information, such as purple for bivalent chromatin and gray for repressed polycomb. Supplemental Figure 9 provides details. Only 10 CpG sites among the 649 array probes corresponding to *PRDM16* exhibited significant differences in methylation according to *PRDM16* expression levels. (D) TSSs of *SCHIP1* in which 4 CpG sites were included in the 244 CpG sites opened specifically in the 2 AMLs with high *PRDM16* expression.

In summary, we successfully classified pediatric AML in accordance with characteristics of molecular biology by studying the DNA methylation levels of extracted CpG sites. Furthermore, from the methylation differences between AML with *FLT3*-ITD with and without high expression of *PRDM16*, we identified TF-binding sites of *STAT5* and *AP-1*, which may be specifically involved in aberrant cell signaling. Targeting molecules for cytogenetically specific AML may facilitate the decision of which drugs to administer. Finally, we confirmed that the methylation pattern drastically changed between high and low *PRDM16* expression. The results of ATAC-seq supported that hypomethylation was associated with high chromatin accessibility and corresponding gene expression, especially of *HOXB* genes, *SCHIP1*, and *PRDM16*. Our findings suggest that DNA methylation plays a key role in leukemogenesis and serves as a useful novel biomarker of pediatric AML.

Acknowledgments

The authors acknowledge the ENCODE Consortium and the ENCODE production laboratories, Bradley Bernstein laboratory (Broad Institute), Richard Myers laboratory (HudsonAlpha Institute for Biology), Vishwanath Iyer laboratory (University of Texas at Austin), John Stamatoyannopoulos laboratory (University of Washington), and Michael Snyder laboratory (Stanford University). The authors also thank Enago for English language review.

This work was supported by Grants-in-Aid for Scientific Research and Exploratory Research from the Ministry of Education, Culture, Sports, Science, and Technology of Japan (16K20951

[N.S.] and 20K17414 [G.Y.]) and by the Practical Research for Innovative Cancer Control from Japan Agency for Medical Research and Development (AMED_15ck0106066h0002, JP16ck0106064, JP19ck0106329, and 19ek0109348s0102; Y. Hayashi).

Authorship

Contribution: G.Y., T. Kawai, and N.S. wrote the paper; G.Y., T. Kawai, N.S., J.I., Y. Hara, K.O., S.-I.T., T. Kaburagi, and K.Y. performed the experiments; G.Y., T. Kawai, N.S., M.S., H.A., S.O., and K. Hata analyzed the data and results; N.K., D.T., A.S., S.A., T.T., and K. Horibe collected the data and samples; Y.S. and S.M. developed the bioinformatic tools; Y. Hayashi designed the study and supervised the work; and all authors critically reviewed and revised the manuscript.

Conflict-of-interest disclosure: The authors declare no competing financial interests.

ORCID profiles: G.Y., 0000-0003-4000-0753; T.K., 0000-0001-8137-0334; D.T., 0000-0003-1520-7007; K. Horibe, 0000-0002-6251-6059; S.O., 0000-0002-7778-5374; K. Hata, 0000-0002-7809-7637.

Correspondence: Yasuhide Hayashi, Institute of Physiology and Medicine, Jobu University, 270-1 Shinmachi, Takasaki, 370-1393 Gunma, Japan; e-mail: hayashiy@jobu.ac.jp.

References

1. Marcucci G, Haferlach T, Döhner H. Molecular genetics of adult acute myeloid leukemia: prognostic and therapeutic implications. *J Clin Oncol*. 2011;29(5):475-486.
2. Pui CH, Carroll WL, Meshinchi S, Arceci RJ. Biology, risk stratification, and therapy of pediatric acute leukemias: an update. *J Clin Oncol*. 2011; 29(5):551-565.
3. Jo A, Mitani S, Shiba N, et al. High expression of *EVI1* and *MEL1* is a compelling poor prognostic marker of pediatric AML. *Leukemia*. 2015;29(5): 1076-1083.
4. Shiba N, Ohki K, Kobayashi T, et al. High *PRDM16* expression identifies a prognostic subgroup of pediatric acute myeloid leukaemia correlated to *FLT3*-ITD, *KMT2A*-PTD, and *NUP98*-*NSD1*: the results of the Japanese Paediatric Leukaemia/Lymphoma Study Group AML-05 trial. *Br J Haematol*. 2016;172(4):581-591.
5. Jiang Y, Dunbar A, Gondek LP, et al. Aberrant DNA methylation is a dominant mechanism in MDS progression to AML. *Blood*. 2009;113(6): 1315-1325.
6. Wilop S, Fernandez AF, Jost E, et al. Array-based DNA methylation profiling in acute myeloid leukaemia. *Br J Haematol*. 2011;155(1):65-72.
7. Ley TJ, Miller C, Ding L, et al; Cancer Genome Atlas Research Network. Genomic and epigenomic landscapes of adult de novo acute myeloid leukemia [published correction appears in *N Engl J Med*. 2013;369(1):98]. *N Engl J Med*. 2013;368(22):2059-2074.
8. Qu X, Othus M, Davison J, et al. Prognostic methylation markers for overall survival in cytogenetically normal patients with acute myeloid leukemia treated on SWOG trials. *Cancer*. 2017;123(13):2472-2481.
9. Lamba JK, Cao X, Raimondi S, et al. DNA methylation clusters and their relation to cytogenetic features in pediatric AML. *Cancers (Basel)*. 2020; 12(10):3024.
10. Li Y, Zhu J, Tian G, et al. The DNA methylome of human peripheral blood mononuclear cells. *PLoS Biol*. 2010;8(11):e1000533.
11. Cecotka A, Polanska J. Region-specific methylation profiling in acute myeloid leukemia. *Interdiscip Sci*. 2018;10(1):33-42.
12. Tokumasu M, Murata C, Shimada A, et al. Adverse prognostic impact of *KIT* mutations in childhood CBF-AML: the results of the Japanese Pediatric Leukemia/Lymphoma Study Group AML-05 trial. *Leukemia*. 2015;29(12):2438-2441.
13. Assenov Y, Müller F, Lutsik P, Walter J, Lengauer T, Bock C. Comprehensive analysis of DNA methylation data with RnBeads. *Nat Methods*. 2014; 11(11):1138-1140.

14. Buenrostro JD, Giresi PG, Zaba LC, Chang HY, Greenleaf WJ. Transposition of native chromatin for fast and sensitive epigenomic profiling of open chromatin, DNA-binding proteins and nucleosome position. *Nat Methods*. 2013;10(12):1213-1218.
15. Corces MR, Trevino AE, Hamilton EG, et al. An improved ATAC-seq protocol reduces background and enables interrogation of frozen tissues. *Nat Methods*. 2017;14(10):959-962.
16. Xu F, Taki T, Yang HW, et al. Tandem duplication of the FLT3 gene is found in acute lymphoblastic leukaemia as well as acute myeloid leukaemia but not in myelodysplastic syndrome or juvenile chronic myelogenous leukaemia in children. *Br J Haematol*. 1999;105(1):155-162.
17. Pabst T, Mueller BU, Zhang P, et al. Dominant-negative mutations of CEBPA, encoding CCAAT/enhancer binding protein-alpha (C/EBPalpha), in acute myeloid leukemia. *Nat Genet*. 2001;27(3):263-270.
18. Taketani T, Taki T, Sugita K, et al. FLT3 mutations in the activation loop of tyrosine kinase domain are frequently found in infant ALL with MLL rearrangements and pediatric ALL with hyperdiploidy. *Blood*. 2004;103(3):1085-1088.
19. Suzuki T, Kiyoi H, Ozeki K, et al. Clinical characteristics and prognostic implications of NPM1 mutations in acute myeloid leukemia. *Blood*. 2005;106(8):2854-2861.
20. Paschka P, Marcucci G, Ruppert AS, et al; Cancer and Leukemia Group B. Adverse prognostic significance of KIT mutations in adult acute myeloid leukemia with inv(16) and t(8;21): a Cancer and Leukemia Group B Study. *J Clin Oncol*. 2006;24(24):3904-3911.
21. Shimada A, Taki T, Tabuchi K, et al. KIT mutations, and not FLT3 internal tandem duplication, are strongly associated with a poor prognosis in pediatric acute myeloid leukemia with t(8;21): a study of the Japanese Childhood AML Cooperative Study Group. *Blood*. 2006;107(5):1806-1809.
22. Matsuo H, Yoshida K, Fukumura K, et al. Recurrent CCND3 mutations in MLL-rearranged acute myeloid leukemia. *Blood Adv*. 2018;2(21):2879-2889.
23. Basecke J, Whelan JT, Griesinger F, Bertrand FE. The MLL partial tandem duplication in acute myeloid leukaemia. *Br J Haematol*. 2006;135(4):438-449.
24. Hollink IH, van den Heuvel-Eibrink MM, Arentsen-Peters ST, et al. NUP98/NSD1 characterizes a novel poor prognostic group in acute myeloid leukemia with a distinct HOX gene expression pattern. *Blood*. 2011;118(13):3645-3656.
25. Shimada A, Iijima-Yamashita Y, Tawa A, et al. Risk-stratified therapy for children with FLT3-ITD-positive acute myeloid leukemia: results from the JPLSG AML-05 study. *Int J Hematol*. 2018;107(5):586-595.
26. Shiba N, Yoshida K, Hara Y, et al. Transcriptome analysis offers a comprehensive illustration of the genetic background of pediatric acute myeloid leukemia. *Blood Adv*. 2019;3(20):3157-3169.
27. Heinz S, Benner C, Spann N, et al. Simple combinations of lineage-determining transcription factors prime cis-regulatory elements required for macrophage and B cell identities. *Mol Cell*. 2010;38(4):576-589.
28. Kanda Y. Investigation of the freely available easy-to-use software 'EZR' for medical statistics. *Bone Marrow Transplant*. 2013;48(3):452-458.
29. Matsuo H, Kajihara M, Tomizawa D, et al. EVI1 overexpression is a poor prognostic factor in pediatric patients with mixed lineage leukemia-AF9 rearranged acute myeloid leukemia. *Haematologica*. 2014;99(11):e225-e227.
30. Kobayashi H, Sakurai T, Imai M, et al. Contribution of intragenic DNA methylation in mouse gametic DNA methylomes to establish oocyte-specific heritable marks. *PLoS Genet*. 2012;8(1):e1002440.
31. Assi SA, Imperato MR, Coleman DJL, et al. Subtype-specific regulatory network rewiring in acute myeloid leukemia. *Nat Genet*. 2019;51(1):151-162.
32. Moore JE, Purcaro MJ, Pratt HE, et al; ENCODE Project Consortium. Expanded encyclopaedias of DNA elements in the human and mouse genomes. *Nature*. 2020;583(7818):699-710.
33. Davis CA, Hitz BC, Sloan CA, et al. The Encyclopedia of DNA elements (ENCODE): data portal update. *Nucleic Acids Res*. 2018;46(D1):D794-D801.
34. Stinson S, Lackner MR, Adai AT, et al. miR-221/222 targeting of trichorhinophalangeal 1 (TRPS1) promotes epithelial-to-mesenchymal transition in breast cancer. *Sci Signal*. 2011;4(186):pt5.
35. Bolouri H, Farrar JE, Triche T Jr, et al. The molecular landscape of pediatric acute myeloid leukemia reveals recurrent structural alterations and age-specific mutational interactions [published corrections appear in *Nat Med*. 2018;24(4):526 and *Nat Med*. 2019;25(3):530]. *Nat Med*. 2018;24(1):103-112.
36. Hayakawa F, Towatari M, Kiyoi H, et al. Tandem-duplicated Flt3 constitutively activates STAT5 and MAP kinase and introduces autonomous cell growth in IL-3-dependent cell lines. *Oncogene*. 2000;19(5):624-631.
37. Giacomelli B, Wang M, Cleary A, et al. DNA methylation epitypes highlight underlying developmental and disease pathways in acute myeloid leukemia. *Genome Res*. 2021;31(5):747-761.
38. Mochizuki N, Shimizu S, Nagasawa T, et al. A novel gene, MEL1, mapped to 1p36.3 is highly homologous to the MDS1/EVI1 gene and is transcriptionally activated in t(1;3)(p36;q21)-positive leukemia cells. *Blood*. 2000;96(9):3209-3214.
39. Pinheiro I, Margueron R, Shukeir N, et al. Prdm3 and Prdm16 are H3K9me1 methyltransferases required for mammalian heterochromatin integrity. *Cell*. 2012;150(5):948-960.
40. Corrigan DJ, Luchsinger LL, Justino de Almeida M, Williams LJ, Strikoudis A, Snoeck H-W. PRDM16 isoforms differentially regulate normal and leukemic hematopoiesis and inflammatory gene signature. *J Clin Invest*. 2018;128(8):3250-3264.
41. Hu T, Morita K, Hill MC, et al. PRDM16s transforms megakaryocyte-erythroid progenitors into myeloid leukemia-initiating cells. *Blood*. 2019;134(7):614-625.

42. Chen WV, Delrow J, Corrin PD, Frazier JP, Soriano P. Identification and validation of PDGF transcriptional targets by microarray-coupled gene-trap mutagenesis. *Nat Genet.* 2004;36(3):304-312.
43. Schmahl J, Raymond CS, Soriano P. PDGF signaling specificity is mediated through multiple immediate early genes. *Nat Genet.* 2007;39(1):52-60.
44. Yang Y, Lin H, Du Z, et al. Imatinib therapy in acute myeloid leukemia with DEK-NUP214 and FIP1L1-PDGFR α rearrangement: a case report. *Oncol Lett.* 2020;19(5):3587-3592.
45. Campregher PV, Halley NDS, Vieira GA, et al. Identification of a novel fusion TBL1XR1-PDGFR β in a patient with acute myeloid leukemia harboring the DEK-NUP214 fusion and clinical response to dasatinib. *Leuk Lymphoma.* 2017;58(12):2969-2972.